Surpassing protein specificity in biomimetics of bacterial amyloids

Julieta M. Sanchez [1,2,3,4¥], Eric Voltà-Durán [1,2,5¥*], Eloi Parladé [1,2,5], Ramón Mangues [2,6], Antonio Villaverde [1,2,5*] Esther Vázquez [1,2,5], Ugutz Unzueta [2,5,6*]

[1] Institut de Biotecnologia i de Biomedicina (IBB), Universitat Autònoma de Barcelona, Barcelona, Spain.

[2] Centro de Investigación Biomédica en Red de Bioingeniería, Biomateriales y Nanomedicina, Instituto de Salud Carlos III, Barcelona, Spain.

[3] Departamento de Química, Cátedra de Química Biológica, Facultad de Ciencias Exactas, Físicas y Naturales, ICTA, Universidad Nacional de Córdoba, Av. Vélez Sársfield 1611, Córdoba 5016, Argentina

[4] Instituto de Investigaciones Biológicas y Tecnológicas (IIByT), CONICET-Universidad Nacional de Córdoba, Córdoba 5016, Argentina

[5] Departament de Genètica i de Microbiologia, Universitat Autònoma de Barcelona, Barcelona, Spain.

[6] Biomedical Research Institute Sant Pau (IR Sant Pau), Barcelona, Spain.

* Correspondence: EV-D, eric.volta@uab.cat; AV, antonio.villaverde@uab.cat; UU, uunzueta@santpau.cat

[¥] Equally contributed

KEYWORDS Recombinant protein; microparticles; amyloids; biomimetics; protein materials

Abstract

In nature, nontoxic protein amyloids serve as dynamic, protein-specific depots, exemplified by both bacterial inclusion bodies and secretory granules from the endocrine system. Inspired by these systems, chemically defined and regulatory-compliant artificial protein microgranules have been developed for clinical applications as endocrine-like protein repositories. This has been achieved by exploiting the reversible coordination between histidine residues and divalent cations such as Zn^{+2}, that promotes protein-protein interactions. While stereospecificity is a main architectonic feature of natural amyloids, the potential for synthetic approaches to create hybrid protein materials remains unexplored. Such materials could enable the occurrence and synchronized local application of diverse proteins in predefined molar ratios, for coupled enzymatic reactions or delivery of synergistically acting polypeptides. Here, we report on the fabrication of artificial protein granules with amyloidal architecture formed by combining two structurally distinct polypeptides. Specifically, we tested co-aggregation of the pairs GFP/IRFP and GFP/β-galactosidase. The formation of hybrid microparticles was confirmed through FRET and complementary methodologies, demonstrating that the His-Zn clustering technology does not require sequential or structural homologies between aggregating polypeptides. This approach opens new avenues for the development of functional depots that capitalize on synergistic protein functionalities, paving the way for next-generation functional materials.

1 Introduction

An important fraction of protein biopharmaceuticals in the market is produced by genetic engineering (namely gene cloning, transfection and expression) in recombinant cells [1–7]. In such biotechnological processes, especially when bacterial cells are used as factories, many of such polypeptides obtained by recombinant DNA technologies fail to reach their native conformation and tend to aggregate as insoluble protein clusters in the cell cytoplasm. Their recovery from cells in soluble versions represents a harsh technological challenge. These protein aggregates, within the microscale, are common in recombinant bacteria and are named inclusion bodies (IBs) [8,9]. IBs, undesired byproducts of recombinant protein production, act as intracellular reservoirs from which polypeptides are steadily released by agents of the quality control system, essentially chaperones, for refolding attempts or proteolysis [10]. Bacterial IBs show an inner structural organization characterized by the occurrence of insoluble, β-sheet-rich fibrils, with a highly ordered, repetitive arrangement of cross-β structures [11,12]. This organization, typically amyloidal, is sustained by stereospecific protein-protein interactions [11,13–15], this fact being a distinctive property of this type of protein materials [13]. Therefore, when two aggregation-prone recombinant proteins are simultaneously produced in bacterial cells, they accumulate in two distinguishable categories of IBs, which are physically separated in the cell cytoplasm [11]. Also, purified IBs can seed, in vitro, the aggregation of homologous but not heterologous protein species that are present in the media as soluble forms [14]. This protein-specific aggregation makes these particles, once separated from producing cells, a relatively pure source of functional proteins ready for refolding or mild extraction [9,16]. Despite such exclusiveness regarding the IB protein species and the consequent tendency to purity in their protein composition, IBs are found associated, once separated from the cell upon cell wall disruption, with bacterial proteins that co-localize in the particles (mainly chaperones and proteases) [17–19]. Other bacterial macromolecules (including nucleic acids and cell wall components) result also attached during purification [20,21]. The co-localizing proteins are excluded from the amyloid core since they are usually trapped in the aggregation process through functional interactions with the misfolding-prone recombinant

protein. Both in physiological buffer and in vivo, IBs release a significant fraction of their forming protein in an active, fully functional form, with application in systemic drug delivery [22,23] but also in regenerative medicine [24] and in enzymatic processes [25]. Therefore, these materials act as mechanically stable but dynamic depots of functional proteins. Despite these promising properties, the unavoidable contamination with native bacterial molecules [17,18,20,21] prevents their further development and use as protein depots or release systems in a biomedical context.

To mimic IB-like properties as functional protein depots, we have designed, fabricated and tested, in different clinical settings, artificial versions of IBs [26,27] suitable for large-scale preparation and handling [28]. For that, His-tagged polypeptides have previously been clustered using coordinating ionic Zn (or other divalent cations) [29]. The resulting microscale granules share amyloidal architecture and protein-releasing properties with both IBs and secretory granules of protein hormones from the mammalian endocrine system [30–35], well characterized mainly in the cases of growth hormone [30,31,34,36] and insulin [36–39]. The structure of those endocrine secretory granules is based on Zn cation as protein-protein clustering agent [30,40–43].

In contrast with the stereospecific constraints of natural amyloid formation, which exclude hybrid protein materials, constructing artificial amyloids from mixed protein species holds significant potential in fields such as enzymology and clinics. Such hybrid platforms would offer a compelling strategy for in situ performance or delivery of synergistically acting proteins at pre-defined molar ratios. However, the capacity of Zn-His coordination to overcome the protein specificity inherent to spontaneous protein aggregation in nature remains unexplored. This study aimed to investigate whether His-tagged polypeptides could co-precipitate in vitro into functional amyloids at the microscale via Zn-His coordination. Using pairs of model polypeptides with distinct structural features, we demonstrated the successful formation of microscale granules composed of multiple protein species, enabled by this simple coordination technology. Inspired by IBs and secretory amyloids in the mammalian endocrine

system, this mechanistically straightforward approach effectively bypasses the protein specificity constraints characteristic of natural aggregation processes.

2 Materials and Methods

2.1 Protein production and characterization

Several structurally unrelated proteins were taken as models for this study, namely green fluorescent protein (GFP-H6), infrared fluorescent protein (iRFP-H6) and the *E. coli* β-galactosidase (β-Gal-H6). The particular iRFP713 variant was selected because of its huge structural differences with the GFP [44]. Genes encoding constructs GFP-H6 and iRFP-H6 were carried in, and expressed from pET22b, whereas pET26b was selected for the production of β-Gal-H6 [45,46]. The hexahistidine tags (H6) were included to allow both affinity-based purification from cell extracts and Zn-mediated cross-protein interactions. The fusion proteins were produced overnight at 20ºC in Lysogeny Broth (LB) medium upon addition of 0.1 mM isopropyl-β-D-1-thiogalactopyranoside. Then, cells were collected by centrifugation (in an Avanti J20XP equipment) at 5,000 *g* for 15 min and resuspended in wash buffer (20 mM Tris, 500 mM NaCl, 10 mM Imidazole, pH 8) in the presence of protease inhibitor (cOmplete™ EDTA-Free, Roche, Basel, Switzerland). Cell lysis was achieved by sonication in a Branson Digital Sonifier (model 102C). The soluble fractions of cell lysates, containing each protein of interest, were separated by centrifugation at 15,000 *g* (Eppendorf Centrifuge 5810R) during 45 min and then loaded onto HisTrap HP columns (Cytiva, Marlborough, MA, USA), for purification by immobilized metal affinity chromatography (IMAC) in an ÄKTA pure system (Cytiva, Marlborough, MA, USA). Protein elution was attained by applying a linear gradient of elution buffer (20 mM Tris, 500 mM NaCl, 500 mM Imidazole, pH 8). Purified protein fractions were then dialyzed and stored in sodium carbonate (166 mM $NaCO_3H$, pH 8) in the case of GFP-H6, saline sodium carbonate (166 mM $NaCO_3H$, 333 mM NaCl, pH 8) for iRFP-H6 and PBS for β-Gal-H6. Sodium carbonate solutions have been previously found to be highly convenient for the stability of proteins and protein aggregates, favoring both manipulation and in vivo administration [26,28,47]. Protein purity and

molecular masses were verified by SDS-PAGE TGX™ gel electrophoresis (Bio-Rad, Hercules, CA, USA) and western blot (WB) using monoclonal anti-GFP antibody (Santa Cruz biotechnology, Inc) for GFP-H6 and anti-His antibody (Clontech Laboratories, Inc) for β-Gal-H6 and iRFP-H6. The images were obtained by a ChemiDoc™ Touch Imaging System, Bio-Rad. Protein concentration was determined by Bradford assay (Bio-Rad, Hercules, CA, USA).

2.2 Protein conjugation with fluorophores

GFP-H6 is a conventional fluorescent protein that requires no modification for fluorescence emission [48]. However, unlike other conventional fluorescent proteins, iRFP713 requires biliverdin (Bv) as a chromophore to become fluorescent. In this process, Bv spontaneously binds to iRFP through a covalent bond [44]. To ensure correct protein conjugation, different Bv/iRFP-H6 mass ratios were tested O/N at 4ºC and the most efficient one selected (Figure S1). β-Gal-H6, a non-fluorescent tetrameric protein [49], was conjugated with N-hydroxysuccinimide (NHS) ester functionalized sulfo-Cyanine 3.5 (Cy 3.5, Lumiprobe, Hannover, Germany), through surface exposed protein lysine-amines. For that, the β-Gal-H6 protein was incubated in presence of an excess of the Cy 3.5 fluorophore (52:1 mass ratio was used, following the manufacturer's standard conjugation protocols for NHS ester labeling) ON at 4ºC.

2.3 Fluorescence properties of soluble proteins

The fluorescence of soluble proteins was determined with a Cary Eclipse spectrofluorometer (Agilent Technologies) in a quartz cell of 2 mm path length. The excitation and the emission slits were set at 5 nm. The excitation wavelengths (λ_{ex}) were 488 nm for GFP-H6, 679 nm for iRFP-H6-Bv and 576 nm for β-Gal -H6-Cy 3.5. Recorded emission wavelengths (λ_{em}) were 512 nm for GFP-H6, 714 nm for iRFP-H6-Bv and 603 nm for β-Gal-H6-Cy 3.5.

2.4 Soluble protein models

Three-dimensional models of GFP-H6, iRFP-H6 and β-Gal-H6 were generated *in silico* using AlphaFold 3 [50]. For 3D structure visualization, ChimeraX software version 1.2 [51] was used.

2.5 Preparation of microparticles

Two types of microparticles (MP) were prepared. Single protein microparticles (sMP) formed by a unique type of protein. Each species, at 0.5 g/L, was incubated with $ZnCl_2$ at 3.5 mM for controlled precipitation. This procedure resulted in the following Zn^{+2}/protein molar ratios: 191 for GFP-H6, 248 for iRFP-H6-Bv and 822 for β-Gal-H6-Cy 3.5. Hybrid protein microparticles (hMP) were generated from a mixture of protein species at 0.5 g/L each, which was incubated with $ZnCl_2$ at 3.5 mM (resulting in the same molar ratios that above, for sMP). The mixtures were gently homogenized and incubated at room temperature for 10 minutes. Then, samples were centrifuged at 15,000 *g* at 4ºC for 15 min and the pellets containing the MPs were stored at -80ºC. A third type of MP sample (mixed single microparticles, mMP) consisted in two different sMP previously formed independently and incubated together.

2.6 Dynamic Light Scattering

The volume size distribution of GFP-H6, iRFP-H6-Bv and β-Gal-H6-Cy 3.5 samples was determined by Dynamic Light Scattering (DLS) at 633 nm and 25°C in a Zetasizer Ultra (Malvern Instruments, Malvern, United Kingdom), using low volume cuvettes. A fluorescence filter was used for iRFP-H6-Bv analysis since its fluorescence spectra interfered with DLS measurement. All measurements were performed in triplicate. Only the most abundant peak (as determined by percent volume) in each measurement was used to calculate average peak sizes. Kruskal-Wallis test was used to determine statistical significance (* indicates $p<0.05$).

2.7 Fourier transform infrared spectroscopy (FT-IR)

Protein MPs were mounted and purged with a continuous N_2 flow, on spectroscopic crystal surfaces. Total Reflectance Spectroscopy was determined 16 times in the form of spectra. A scan rate of 50 cm^{-1}/min with a nominal resolution of 2 cm^{-1} was applied in a Tensor 27 Bruker spectrometer with a Specac's Golden Gate Attenuated Total Reflectance (ATR) accessory. Measurements were always done at 20ºC under an N2 flux. The background was subtracted from the absorbance and the second derivative allowed the identification and analyses of different band components.

Following the previously described procedure, the components were fitted to the original (non-deconvolved) spectrum, assuming a Gaussian shape. Data was treated using the PeakFit 4.1.2 software.

2.8 Förster Resonance Energy Transfer

Two approaches were taken to verify the colocalization of proteins of different nature within the same particle, namely Förster Resonance Energy Transfer (FRET) and confocal microscopy. FRET occurs when the energy of an excited donor fluorophore is transferred in a non-radiative way to a nearby acceptor fluorophore. Here we applied GFP as the donor and iRFP or β-Gal as the acceptors. GFP-H6/iRFP-H6-Bv and GFP-H6/ β-Gal-H6-Cy 3.5 MPs, each containing 0.05 g/L of protein, were resuspended in carbonate solution (166 mM $NaCO_3H$; pH 8) and fluorescence emission spectra were recorded using a Cary Eclipse spectrofluorimeter . For FRET studies, all the samples were excited at 488 nm, which is the excitation wavelength of GFP-H6 (the donor fluorophore) and recorded at the partner protein emission wavelength (603 nm for β-Gal-H6-Cy 3.5 and 714 nm for iRFP-H6-Bv, the acceptor fluorophores). All experiments were performed in triplicate. Data were represented as mean % values ± standard error of the mean (SEM). Normality of data was confirmed by Shapiro-Wilk test. Unpaired t-tests were performed to determine statistical significance. * indicates $p<0.05$.

2.9 Confocal microscopy

For confocal microscopy, around 0.5-1 μg of protein in the form of hMP and mMP were placed on microscope slides and images were captured on an inverted TCS SP5 Spectral confocal microscope (Leica Microsystems) using an oil immersion objective lens (HCX PL APO lambda blue 63.0x1.40 OIL UV). GFP excitation was reached via a 488 nm laser and fluorescence was captured at 500-555 nm. Cy 3.5 excitation was reached via a 561 nm laser, and the fluorescence was captured at 571-700 nm. Multitrack sequential acquisition was used to avoid inter-channel crosstalk. The confocal pinhole was set to 1 Airy unit.

Confocal microscopy colocalization analyses were performed using ImageJ following Manders test [52]. Independent confocal images (n ≥ 7) from each sample were processed and evaluated to determine the percentage of colocalization between both fluorophores. The same threshold rule (50-255) was applied in every image to remove noise. Mean grey values (Analyze tool) were measured for each channel, rendering the amount of red and green positive pixels in each image. Image calculator processing tool (AND) was applied to generate composite images showing positive pixels when both red and green signals were positive for that pixel. Mean gray value of composite images were measured as previously described in [52,53]. For a given image, the percentage of colocalization between red and green fluorescence was calculated as follows:

$$\%\ Colocalization_{R\rightarrow G} = \left(\frac{V_{R+G}}{V_R}\right) \times 100\% \ Colocalization_{G\rightarrow R} = \left(\frac{V_{R+G}}{V_G}\right) \times 100$$

V_{R+G}: Mean grey value of the composite image (red + green channels). V_R: Mean grey value of the red channel. V_G: Mean grey value of the green channel.

Data were represented as mean % values ± standard error of the mean (SEM). Normality of data was confirmed by Shapiro-Wilk and Kolmogorov-Smirnov test. An unpaired t-test was performed to determine statistical significance. ** indicates $p<0.001$.

3 Results

The aim of this study was to evaluate the methodological feasibility of producing hybrid protein granules—mimicking bacterial inclusion bodies—composed of controlled amounts of structurally distinct polypeptides. For that, a His-tagged GFP and fluorophore-conjugated versions of His-tagged iRFP and β-galactosidase (iRFP-H6-Bv and β-Gal-H6-Cy 3.5 respectively) were selected, envisaging a Förster Resonance Energy Transfer (FRET)-based approach. All these proteins (Figure 1A) were produced from plasmid-carrying genes and purified from recombinant *E. coli.* Being proteolytically stable, they showed the expected molecular masses (Figure 1B).

The excitation and emission fluorescence spectra of the GFP-H6/iRFP-H6-Bv and GFP-H6/ β-Gal-H6-Cy 3.5 pairs showed overlapping areas and distinguishable emission curves (Figure 1C,D), enabling FRET-based confirmation of close molecular proximity and hence in potentially hybrid supramolecular complexes. DLS analysis of the protein samples, upon chemical coupling, rendered relatively monodisperse size peaks compatible with monomeric or dimeric disposition of GFP-H6 and iRFP-H6-Bv, and with the tetrameric organization of a functional, native β-galactosidase in the case of β-Gal-H6-Cy 3.5 (Figure 1E).

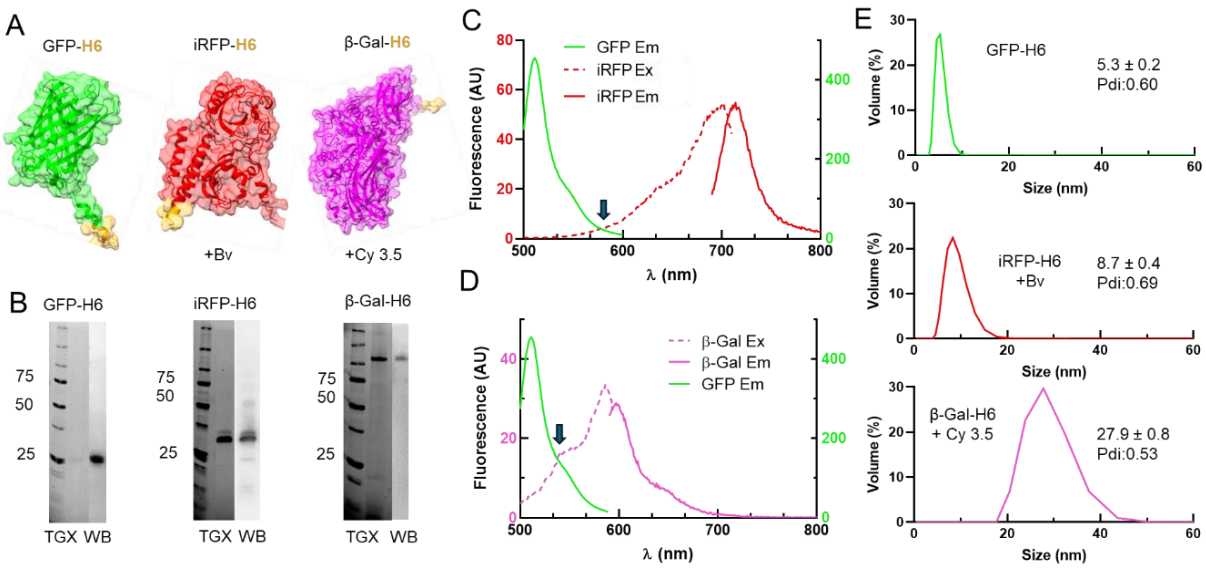

Figure 1. Characterization of soluble protein. A) Three-dimensional structure of fluorescent GFP-H6, fluorophore conjugated iRFP-H6-Bv and β-Gal-H6-Cy 3.5. Bv: biliverdin, Cy 3.5: sulfo-Cyanine 3.5. The solvent-exposed H6 tag is represented in pale orange. B) Purity of fluorescent proteins analyzed by SDS-PAGE electrophoresis (TGX) and Western blot. C) Fluorescence emission (GFP Em) spectra of GFP-H6 (green line) and excitation (iRFP Ex) and emission (iRFP Em) spectra of iRFP-H6-Bv (iRFP,red lines). D) Fluorescence emission spectra of (GFP Em) spectra of GFP-H6 (green line) and excitation (β-Gal Ex) and emission (β-Gal Em) spectra β-Gal-Cy 3.5 (β-Gal) (pink lines). Arrows indicate the spectral overlap. E) Hydrodynamic size of soluble proteins. Data is expressed in nanometers +/- standard error. Pdi: polydispersion index.

At first, we fabricated, in vitro, IB mimetics in the form of Zn-promoted MP as described [26]. This was done by adding ionic Zn at a molar excess of 191-fold for GFP-H6, 248-fold for iRFP-H6-Bv, and 822-fold for β-Gal-H6-Cy 3.5 (0.5 g/L of

protein and 3.5 mM $ZnCl_2$ in all cases), over samples of each of the three single model proteins (Figure 2A,B) as indicated (Figure 2C). In addition, mixtures of GFP-H6 with iRFP-H6-Bv (Figure 2A) and GFP-H6 with β-Gal-H6-Cy 3.5 (Figure 2B) were subjected to Zn-mediated clustering. The resulting hMPs were successfully formed, exhibiting micron dimensions in the range of those of conventional sMPs (Figure 2). The size of the hMP did not appear to be predictable based on those of the sMP formed by their individual components. The moderate error bars in the measurements and the significant differences between the components of tested each pair indicate that particle size is an inherent property of the material, rather than the result of random aggregation. Then, the unexpected size of the hMP suggested that particle size is determined or at least greatly influenced by the specific properties of the building block polypeptide. This is in agreement with previous observations regarding other MP properties such as the nature of the particle core or protein bioavailability [54]. In addition, both sMP and hMP showed amyloid-like conformation at similar extents, ranging from 32 to 48 % (Table 1). Such a similarity is indicative that both components of hMP participate in the amyloid formation.

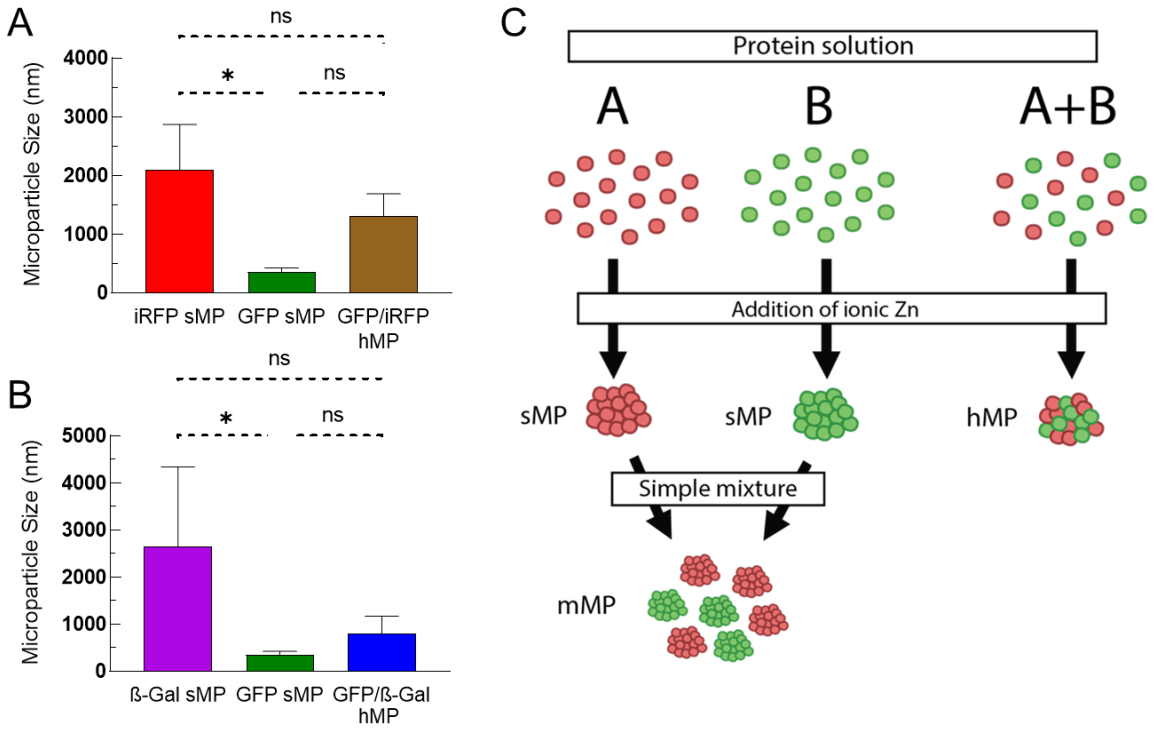

Figure 2. Characterization of protein microparticles. A) Mean volume size of single iRFP-H6-Bv microparticles (iRFP sMP), GFP-H6 microparticles (GFP sMP), and

hybrid GFP-H6 / iRFP-H6-Bv microparticles (GFP/iRFP hMP). B) Mean volume size of single β-Gal-H6-Cy 3.5 microparticles (β-Gal sMP), GFP-H6 microparticles (GFP sMP), and hybrid GFP-H6 / β-Gal-H6-Cy 3.5 microparticles (GFP/ β-Gal hMP). Data were represented as mean % values ± standard error of the mean (SEM) (* indicates $p<0.05$). C) Strategies for the preparation of protein MP. A and B are unrelated protein species, both H6-tagged at the C-terminus.

Table 1. ATR FT-IR analysis of different formats of microparticles.

Protein MP	**Structural rate (%)**			
	Amyloid-like 1628-1632 cm^{-1}	**Unordered 1644-1648 cm^{-1}**	**Alpha helix 1659- 1668 cm^{-1}**	**Beta bands 1678-1681 cm^{-1}**
iRFP sMP	35.3 ± 1.3	33.5 ± 2	27.6 ± 2.4	3.9 ± 0.4
GFP sMP	32.28 ± 1.17	32.65 ± 2.5	24.3 ± 3.10	10.9 ± 1.2
β-Gal sMP	48.3 ± 3.15	-	46.3 ± 1.4	5.3 ± 1.8
GFP/iRFP hMP	46.2 ± 1.4	28.2 ± 1.25	22.5 ± 1.6	3 ± 0.9
GFP/ β-Gal hMP	39.8 ± 0.35	29.7 ± 0.35	26.7 ± 0.6	3.6 ± 0.7

The hypothesis that hMP were formed by combined pairs of different proteins required confirmation. In recombinant bacteria, independent IBs are formed when two heterologous proteins are simultaneously produced by the cell factory machinery [11]. In vitro, independent and exclusive protein clusters might have also been formed upon Zn^{+2} addition, and hMP could be, in fact, a mixture of independent sMP. To discard this possibility, we studied FRET of both the presumed hMP and mixtures, in pairs, of individual sMP (mMP). These mMP were obtained in vitro by simply combining prefabricated sMP composed of the building block proteins (Figure 2C). As shown in Figure 3 A and C, upon GFP (donor fluorophore) excitation the fluorescence signal increase in the samples supposed to be hMP respect to a basal signal of mMP. The fluorescence ratio between acceptor fluorophores (iRFP or β-Gal) and GFP fully highlights the FRET event (Figure 3 B and D). This observation confirms that hMP were formed, as expected, by two different protein species, in contrast with mMP samples that are a mixture of sMPs generated predominantly by a single protein species. Then, unlike bacterial IBs whose formation is protein specific and exclusive [11,14], their biomimetic counterparts, formed by Zn-His coordination, may assume a heterologous composition.

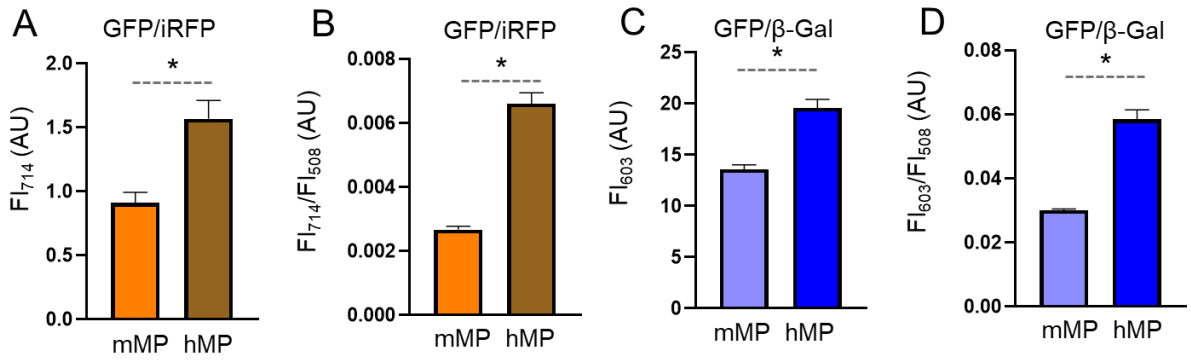

Figure 3. FRET analysis in mixed and hybrid microparticles. A) iRFP-H6-Bv fluorescence emission at 714 nm of mixed GFP/iRFP microparticles (mMP) or hybrid GFP/iRFP microparticles (hMP) upon GFP excitation at 488 nm. B) Rates of iRFP-H6-Bv fluorescence increase (at 714 nm) respect to GFP-H6 fluorescence decrease (at 508 nm) in mixed GFP/iRFP microparticles (mMP) or hybrid GFP/iRFP microparticles (hMP) upon GFP excitation at 488 nm. C) β-Gal-H6-Cy 3.5 fluorescence emission at 603 nm of mixed GFP/ β-Gal microparticles (mMP) or hybrid GFP/β-Gal microparticles (hMP) upon GFP excitation at 488 nm. D) Rates of β-Gal-H6-Cy 3.5 fluorescence increase (at 603 nm) respect to GFP-H6 fluorescence decrease (at 508 nm) in mixed GFP/ β-Gal microparticles (mMP) or hybrid GFP/ β-Gal microparticles (hMP) upon GFP excitation at 488 nm. Data were represented as mean % values ± standard error of the mean (SEM). * indicates $p<0.05$. Note the different Y scale ranges in the pairs GFP/iRFP and GFP/ β-Gal, resulting from the different spectral overlaps shown in Figure 1 C,D.

Even though the FRET data was robust and conclusive in the context of mMP and hMP comparison, we wanted to double-check the heterogeneous nature of hMP visually, by confocal microscopy, using samples of already formed MP. Control sMP of GFP-H6 and β-Gal-H6-Cy 3.5 showed exclusive green (GFP) or red (Cy 3.5) fluorescence as expected (Figure 4A, top). However, amerging between green and red channels (represented in yellow) was observed in the pair of GFP-H6 / β-Gal-H6-Cy 3.5 hMP but not in samples of their corresponding mMP version (Figure 4A, bottom), verifying a spatial overlap of emission signals of GFP and Cy 3.5. The quantitative analysis of the merging signal (Figure 4B, bottom) fully confirmed the hybrid nature of hMP through the high degree of signal colocalization.

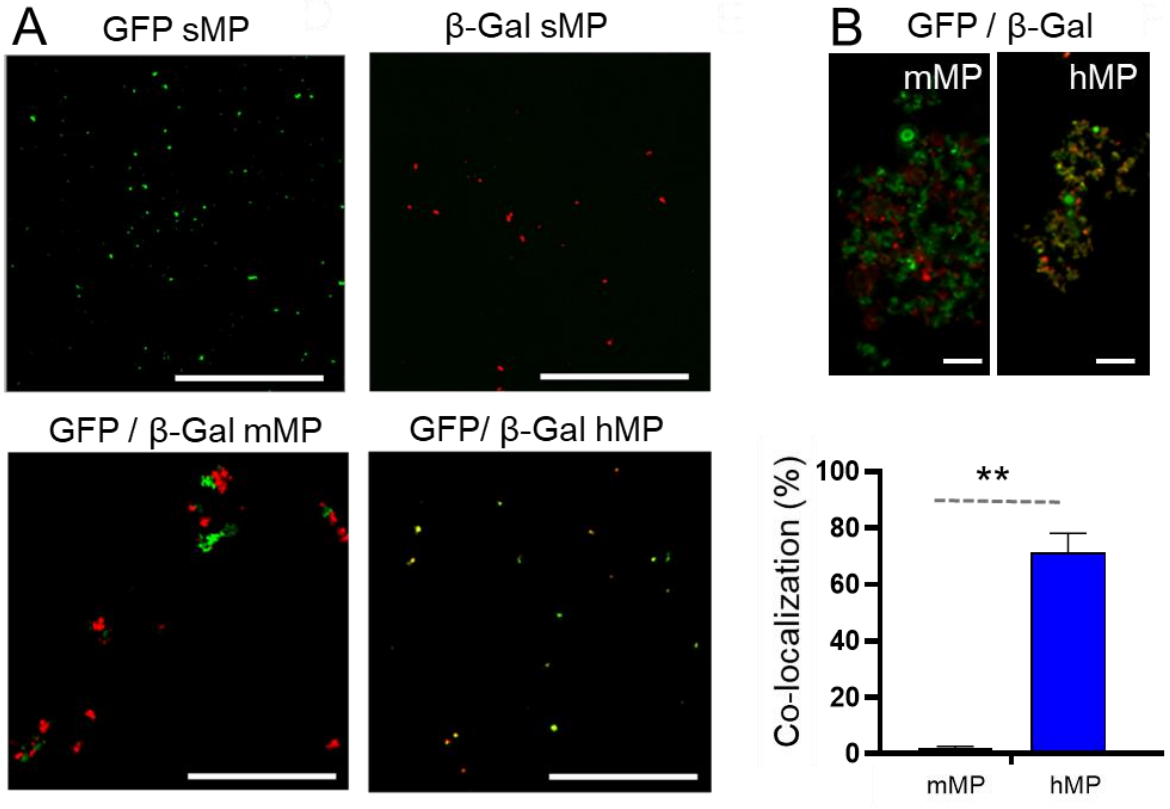

Figure 4. Confocal microscopy analysis of GFP/β-Gal Microparticles. A) Representative images of single GFP-H6 microparticles (GFP sMP), single β-Gal -H6-Cy 3.5 microparticles (β-Gal sMP), mixed GFP-H6 / β-Gal-H6-Cy 3.5 microparticles (GFP/β-Gal mMP) and hybrid GFP-H6 / β-Gal -H6-Cy 3.5 microparticles (GFP/β-Gal hMP). GFP-H6 was excited at 488 nm and β-Gal-H6-Cy 3.5 was excited at 561 nm. Bar size: 30 μm. B) Representative images showing the colocalization of GFP-H6 and β-Gal-H6-Cy 3.5 within mixed GFP/β-Gal microparticles (mMP) and hybrid GFP/ β-Gal microparticles (hMP). Scale Bar: 10 μm. Percentage of colocalization is quantified in the graph below (calculated as the colocalization of red signal with green signal). Data were represented as mean % values ± standard error of the mean (SEM). ** indicates $p<0.001$.

4. Discussion

The set of data set presented here fully supports that protein MP formed by Zn-mediated coordination of His-rich proteins are mechanically constructed irrespective of stereospecificity, a requisite that is critical in the formation of natural amyloids such as IBs [11,13,55]. Even both types of materials, synthetic and natural, show a similar extent of amyloidal architecture (around 40 %, see Table 1 and [56]), the category of patches that support protein-protein contacts are essentially different. In

mammalian secretory granules, which also exhibit amyloid-like organization, only a subset of the involved proteins participates in the amyloid structure [36], a fact that might be also true in bacterial inclusion bodies since an important population of the embedded protein is biologically active [9,57]. The Zn-His coordination, especially when the His-rich region is a terminal polyhistidine such as H6, far from any functional domain, may be a precise molecular driver for protein cross-interaction and further aggregation in absence of stereospecific contacts. Then, the Zn-His-assisted protein aggregation is able to produce artificial IB mimetics that in contrast to their natural counterparts [11,14], can be formed by heterologous proteins at defined ratios provided they are conveniently tagged with anchoring His-rich domains. How Zn-His coordination triggers amyloidogenesis is only partially understood [58–60]. However, this event provides an extremely efficient approach for the simple, fast and controlled generation of functional, microscale, protein materials by simple fabrication procedures.,

Irrespective of the precise mechanics, the approach presented here opens a gate to explore applicability of hybrid protein depots in different clinical or industrial settings in which different polypeptides need to combine their biologic activities at defined ratios and in very local environments. Considering traditional strategies for protein immobilization, such as affinity-tagged approaches or chemical crosslinking, they are often limited by product specificity and harsh reaction conditions, that tend to disrupt protein functionality [61–63]. Also, while some smart approaches such as CLEAs [64] result in only moderate loss of protein activities, the cross-linking processes might be not (or hardly) reversible. In comparison, Zn-mediated aggregation provides a mild, sequence-independent platform for generating stable, functional aggregates with broad utility and with potential for controlled disintegration and protein release under physiological conditions. Furthermore, other recently developed mild approaches for the generation of immobilized multiprotein systems, also based on the use of ionic Zn as a crosslinking agent, are methodologically more complex than simple protein aggregation [65]. Interestingly, His-tagging is a common procedure in protein biotechnology, since His-rich peptides such as H6, also serve as protein purification tags for affinity chromatography [66]. Therefore, many relevant proteins of industrial

or pharmaceutical interest have been already produced and are available in H6-tagged forms. It must be stressed that in comparison to methods to force protein co-aggregation in vivo (eg. in the bacterial cytoplasm [67]), the formation of synthetic amyloids with hybrid composition as described here benefits from the use of pure, perfectly characterized protein as starting material. This fact ensures fine quality control of the products and a smooth regulatory route towards clinical applications.

Zn-mediated protein aggregation not only promotes the controlled formation of mechanically stable amyloid structures but also ensures that the proteins retain their functional properties. This unique combination of structural robustness, provided by the amyloidal subpopulation, and functional preservation, makes this simple approach ideal for diverse applications, from biocatalysis to material science. Importantly, the process is fully reversible as Zn is removed from the aggregates, either forced by chelating agents [68] or by simple diffusion in vivo, upon administration [26,47]. The data presented in this study validates an emerging methodology, but it also highlights its capability to bypass the constraints of sequence homology and stereospecific interactions inherent in natural systems. The versatility and simplicity of this approach to generate functional protein depots out of diverse polypeptides, open new avenues for its application in biotechnological and material science fields, offering a robust alternative to existing protein immobilization strategies.

5. Conclusions

Unlike bacterial inclusion bodies, natural amyloidal protein depots found in recombinant bacteria, their mimetic materials fabricated in vitro through Zn-His coordination do not require specific protein-protein interactions to be formed. That allows the construction of granular depots, at the microscale, made of controlled mixtures of different protein species at defined ratios. Sharing both type of materials a similar amyloidal content (around 40 %), the Zn-His coordination approach allows mechanically stable cross-molecular contacts without the constraint of sequence homology, thus opening a versatile route for the design and construction of protein

microscale materials, that formed by heterologous building blocks, should show complex functionalities.

Supplementary Figures

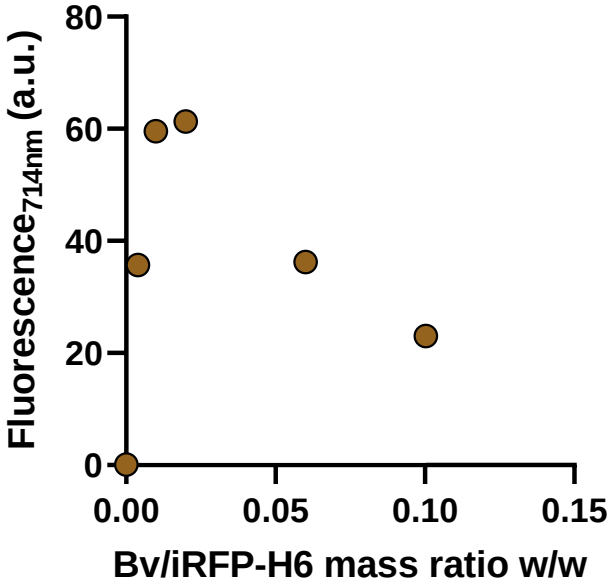

Figure S1. Fluorescence emission of iRFP-H6 (iRFP) bound to biliverdine (Bv) at 714 nm as a function of Bv/iRFP mass ratio. A mass ratio Bv/iRFP=0.02 was chosen for the fluorescence analysis.

Acknowledgments: We appreciate the support from AEI for the development of multimeric recombinant drugs (mainly PID2022-1368450 OB-10/AEI/10.13039/501100011033 to AV and EV but also PID2019-105416RB-I00/AEI/10.13039/501100011033 and PDC2022-133858-I00 to E.V.,) and to Instituto de Salud Carlos III (PI20/00400 and PI23/00318 to U.U.) co-funded by European Regional Development Fund (ERDF, a way to make Europe). JMS is supported with a María Zambrano postdoctoral researcher contract (677904) from Ministerio de Universidades and European Union ("Financed by European Union-Next GenerationEU"). The authors also appreciate the financial support received from AGAUR (2021SGR00092 to A.V.), from CIBER -Consorcio Centro de Investigación Biomédica en Red- (CB06/01/0014 and CB06/01/1031), and from Instituto de Salud Carlos III, Ministerio de Ciencia e Innovación, through intramural projects (NANO4CANCER to A.V., NANOREMOTE to E.V. and NANOSCAPE to U.U). U.U. is supported by a Miguel Servet contract (CP19/00028) from ISCIII co-funded by

European Social Fund (ESF investing in your future). We also acknowledge the support from the ICTS "NANBIOSIS", more specifically from the Protein Production Platform of CIBER in Bioengineering, Biomaterials & Nanomedicine (CIBER-BBN)/ IBB, at the UAB (http://www.nanbiosis.es/portfolio/u1-protein-production-platform-ppp/). Molecular graphics and analyses performed with UCSF ChimeraX, developed by the Resource for Biocomputing, Visualization, and Informatics at the University of California, San Francisco, with support from National Institutes of Health R01-GM129325 and the Office of Cyber Infrastructure and Computational Biology, National Institute of Allergy and Infectious Diseases. Fluorescence spectroscopy results were aquired at the Servei of Luminescència i Espectroscòpia de Biomolècules (UAB) and Confocal microscopy images were obtained at the Servei de Microscòpia i Difracció de Raigs X (UAB).

Data Availability: Raw data from the experimental can be found here: https://doi.org/10.34810/data1773

CRediT authorship contribution statement Julieta M. Sánchez: Writing – review & editing, Methodology, Investigation. **Eric Voltà-Durán:** Writing – review & editing, Methodology, Investigation. **Eloi Parladé:** Writing – review & editing, Methodology, Investigation. **Ramón Mangues:** Funding acquisition, Conceptualization. **Antonio Villaverde:** Writing – original draft, Supervision, Resources, Conceptualization. **Esther Vázquez:** Writing – review & editing, Supervision, Project administration, Funding acquisition, Conceptualization. **Ugutz Unzueta:** Writing – review & editing, Supervision, Methodology, Conceptualization.

Conflicts of Interest: The authors declare the following financial interests/personal relationships which may be considered as potential competing interests: JMS, RM, AV and EV have a patent application PROTEIN NANO OR MICROPARTICLES AS ARTIFICIAL INCLUSION BODIES (PCT/EP2020/059994) under negotiation for license. The other authors declare that they have no known competing financial interests or personal relationships that could have appeared to influence the work reported in this paper.

References

[1] D. Agyei, I. Ahmed, Z. Akram, H. M. N. Iqbal, M. K. Danquah, Protein and Peptide Biopharmaceuticals: An Overview, Protein Pept Lett 24 (2017). https://doi.org/10.2174/0929866523666161222150444.

[2] T.K. Ha, J.S. Lee, G.M. Lee, Platform Technology for Therapeutic Protein Production, in: Cell Culture Engineering, 2019. https://doi.org/10.1002/9783527811410.ch1.

[3] S. Mitragotri, P.A. Burke, R. Langer, Overcoming the challenges in administering biopharmaceuticals: Formulation and delivery strategies, Nat Rev Drug Discov 13 (2014). https://doi.org/10.1038/nrd4363.

[4] A. Mizukami, A.L. Caron, V. Picanço-Castro, K. Swiech, Platforms for recombinant therapeutic glycoprotein production, in: Methods in Molecular Biology, 2018. https://doi.org/10.1007/978-1-4939-7312-5_1.

[5] L.A. Palomares, S. Estrada-Mondaca, O.T. Ramírez, Production of recombinant proteins: challenges and solutions., Methods Mol Biol 267 (2004). https://doi.org/10.1385/1-59259-774-2:015.

[6] S.R. Schmidt, Fusion-proteins as biopharmaceuticals - Applications and challenges, Curr Opin Drug Discov Devel 12 (2009).

[7] P.S. Slathia, Sagrika, E. Sharma, I.A. Khan, R.S. Thakur, P. Sharma, Recombinant Production of Therapeutic Proteins, in: Protein-Based Therapeutics, 2023. https://doi.org/10.1007/978-981-19-8249-1_4.

[8] A. Ramón, M. Señorale-Pose, M. Marín, Inclusion bodies: Not that bad..., Front Microbiol 5 (2014). https://doi.org/10.3389/fmicb.2014.00056.

[9] P. Singhvi, A. Saneja, S. Srichandan, A.K. Panda, Bacterial Inclusion Bodies: A Treasure Trove of Bioactive Proteins, Trends Biotechnol 38 (2020). https://doi.org/10.1016/j.tibtech.2019.12.011.

[10] S. Ventura, A. Villaverde, Protein quality in bacterial inclusion bodies, Trends Biotechnol 24 (2006) 179–185.

[11] M. Morell, R. Bravo, A. Espargaró, X. Sisquella, F.X. Avilés, X. Fernàndez-Busquets, S. Ventura, Inclusion bodies: Specificity in their aggregation process and amyloid-like structure, Biochim Biophys Acta Mol Cell Res 1783 (2008). https://doi.org/10.1016/j.bbamcr.2008.06.007.

[12] L. Wang, Towards revealing the structure of bacterial inclusion bodies., Prion 3 (2009). https://doi.org/10.4161/pri.3.3.9922.

[13] M.A. Speed, D.I.C. Wang, J. King, Specific Aggregation of Partially Folded Polypeptide Chains: The Molecular Basis of Inclusion Body Composition, Nat Biotechnol 14 (1996). https://doi.org/10.1038/nbt1096-1283.

[14] M. Carrió, N. González-Montalbán, A. Vera, A. Villaverde, S. Ventura, Amyloid-like properties of bacterial inclusion bodies, J Mol Biol 347 (2005). https://doi.org/10.1016/j.jmb.2005.02.030.

[15] E. García-Fruitõs, R. Sabate, N.S. De Groot, A. Villaverde, S. Ventura, Biological role of bacterial inclusion bodies: A model for amyloid aggregation, FEBS Journal 278 (2011). https://doi.org/10.1111/j.1742-4658.2011.08165.x.

[16] S.M. Singh, A.K. Panda, Solubihzation and refolding of bacterial inclusion body proteins, J Biosci Bioeng 99 (2005). https://doi.org/10.1263/jbb.99.303.

[17] U. Rinas, T.C. Boone, J.E. Bailey, Characterization of inclusion bodies in recombinant Escherichia coli producing high levels of porcine somatotropin, J Biotechnol 28 (1993). https://doi.org/10.1016/0168-1656(93)90179-Q.

[18] R.A. Hart, U. Rinas, J.E. Bailey, Protein composition of Vitreoscilla hemoglobin inclusion bodies produced in Escherichia coli, Journal of Biological Chemistry 265 (1990). https://doi.org/10.1016/s0021-9258(19)38405-4.

[19] M.M. Carrió, A. Villaverde, Localization of chaperones DnaK and GroEL in bacterial inclusion bodies, J Bacteriol 187 (2005) 3599–3601. https://doi.org/10.1128/JB.187.10.3599-3601.2005.

[20] B. Jürgen, A. Breitenstein, V. Urlacher, K. Büttner, H. Lin, M. Hecker, T. Schweder, P. Neubauer, Quality control of inclusion bodies in Escherichia coli, Microb Cell Fact 9 (2010). https://doi.org/10.1186/1475-2859-9-41.

[21] N.N. Mohamad Alias, E.B. Beng Ong, M.W.O. Liew, Removal and monitoring of residual nucleic acids from core streptavidin inclusion bodies for increased refolding yield, Protein Expr Purif 225 (2025) 106591. https://doi.org/10.1016/j.pep.2024.106591.

[22] M.V. Céspedes, Y. Fernández, U. Unzueta, R. Mendoza, J. Seras-Franzoso, A. Sánchez-Chardi, P. Álamo, V. Toledo-Rubio, N. Ferrer-Miralles, E. Vázquez, S. Schwartz, I. Abasolo, J.L. Corchero, R. Mangues, A. Villaverde, Bacterial mimetics of endocrine secretory granules as immobilized in vivo depots for functional protein drugs, Sci Rep 6 (2016). https://doi.org/10.1038/srep35765.

[23] M.V. Céspedes, O. Cano-Garrido, P. Álamo, R. Sala, A. Gallardo, N. Serna, A. Falgàs, E. Voltà-Durán, I. Casanova, A. Sánchez-Chardi, H. López-Laguna, L. Sánchez-García, J.M. Sánchez, U. Unzueta, E. Vázquez, R. Mangues, A. Villaverde, Engineering Secretory Amyloids for Remote and Highly Selective Destruction of Metastatic Foci, Advanced Materials 32 (2020). https://doi.org/10.1002/adma.201907348.

[24] J. Seras-Franzoso, K. Peebo, J. Luis Corchero, P.M. Tsimbouri, U. Unzueta, U. Rinas, M.J. Dalby, E. Vazquez, E. García-Fruitós, A. Villaverde, A Nanostructured Bacterial

Bioscaffold for The Sustained Bottom-Up Delivery of Protein Drugs, Nanomedicine 8 (2013) 1587–1599. https://doi.org/10.2217/nnm.12.188.

[25] U. Rinas, E. Garcia-Fruitós, J.L. Corchero, E. Vázquez, J. Seras-Franzoso, A. Villaverde, Bacterial Inclusion Bodies: Discovering Their Better Half, Trends Biochem Sci 42 (2017). https://doi.org/10.1016/j.tibs.2017.01.005.

[26] J.M. Sánchez, H. López-Laguna, E. Parladé, A. Di Somma, A.L. Livieri, P. Álamo, R. Mangues, U. Unzueta, A. Villaverde, E. Vázquez, Structural Stabilization of Clinically Oriented Oligomeric Proteins During their Transit through Synthetic Secretory Amyloids, Advanced Science (2024). https://doi.org/10.1002/advs.202309427.

[27] J.M. Sánchez, H. López-Laguna, P. Álamo, N. Serna, A. Sánchez-Chardi, V. Nolan, O. Cano-Garrido, I. Casanova, U. Unzueta, E. Vazquez, R. Mangues, A. Villaverde, Artificial Inclusion Bodies for Clinical Development, Advanced Science 7 (2020). https://doi.org/10.1002/advs.201902420.

[28] M. TP Favaro, H. López-Laguna, E. Voltà-Durán, L. Alba-Castellon, J.M. Sánchez, I. Casanova, U. Unzueta, R. Mangues, A. Villaverde, E. Vázquez, Lyophilization of biomimetic amyloids preserves their regulatable, endocrine-like functions for nanoparticle release, Appl Mater Today 39 (2024) 102348. https://doi.org/10.1016/J.APMT.2024.102348.

[29] H. López-Laguna, J. Sánchez, U. Unzueta, R. Mangues, E. Vázquez, A. Villaverde, Divalent Cations: A Molecular Glue for Protein Materials Trends in Biochemical Sciences An official publication of the INTERNATIONAL UNION OF BIOCHEMISTRY AND MOLECUL AR BIOLOGY, Trends Biochem Sci 45 (2020). https://doi.org/10.1016/j.tibs.2020.08.003.

[30] R.S. Jacob, S. Das, S. Ghosh, A. Anoop, N.N. Jha, T. Khan, P. Singru, A. Kumar, S.K. Maji, Amyloid formation of growth hormone in presence of zinc: Relevance to its storage in secretory granules, Scientific Reports 2016 6:1 6 (2016) 1–18. https://doi.org/10.1038/srep23370.

[31] A. Anoop, S. Ranganathan, B. Das Dhaked, N.N. Jha, S. Pratihar, S. Ghosh, S. Sahay, S. Kumar, S. Das, M. Kombrabail, K. Agarwal, R.S. Jacob, P. Singru, P. Bhaumik, R. Padinhateeri, A. Kumar, S.K. Maji, Elucidating the role of disulfide bond on amyloid formation and fibril reversibility of somatostatin-14: Relevance to its storage and secretion, Journal of Biological Chemistry 289 (2014). https://doi.org/10.1074/jbc.M114.548354.

[32] R.S. Jacob, A. Anoop, S.K. Maji, Protein Nanofibrils as Storage Forms of Peptide Drugs and Hormones, Adv Exp Med Biol 1174 (2019) 265–290. https://doi.org/10.1007/978-981-13-9791-2_8/FIGURES/5.

[33] A. Soragni, S.K. Maji, R. Riek, Toward a comprehension of functional aggregation into amyloids in pituitary secretory granules, Amyloid 17 (2010).

[34] S.K. Maji, M.H. Perrin, M.R. Sawaya, S. Jessberger, K. Vadodaria, R.A. Rissman, P.S. Singru, K.P.R. Nilsson, R. Simon, D. Schubert, D. Eisenberg, J. Rivier, P. Sawchenko, W. Vale, R. Riek, Functional amyloids as natural storage of peptide hormones in pituitary secretory granules, Science (1979) 325 (2009) 328–332. https://doi.org/10.1126/SCIENCE.1173155/SUPPL_FILE/MAJI.SOM.PDF.

[35] D. Chatterjee, R.S. Jacob, S. Ray, A. Navalkar, N. Singh, S. Sengupta, L. Gadhe, P. Kadu, D. Datta, A. Paul, A. Sakunthala, S. Mehra, C. Pindi, S. Kumar, P.S. Singru, S. Senapati, S.K. Maji, Co-aggregation and secondary nucleation in the life cycle of human prolactin/galanin functional amyloids, Elife 11 (2022). https://doi.org/10.7554/eLife.73835.

[36] W.C. Hymer, W.J. Kraemer, Resistance exercise stress: theoretical mechanisms for growth hormone processing and release from the anterior pituitary somatotroph, Eur J Appl Physiol 123 (2023). https://doi.org/10.1007/s00421-023-05263-8.

[37] M. Groenning, S. Frokjaer, B. Vestergaard, Formation Mechanism of Insulin Fibrils and Structural Aspects of the Insulin Fibrillation Process, Curr Protein Pept Sci 10 (2009). https://doi.org/10.2174/138920309789352038.

[38] J.L. Jiménez, E.J. Nettleton, M. Bouchard, C. V. Robinson, C.M. Dobson, H.R. Saibil, The protofilament structure of insulin amyloid fibrils, Proc Natl Acad Sci U S A 99 (2002). https://doi.org/10.1073/pnas.142459399.

[39] N. Yamamoto, R. Inoue, Y. Makino, H. Sekiguchi, N. Shibayama, A. Naito, M. Sugiyama, E. Chatani, Tracking the Structural Development of Amyloid Precursors in the Insulin B Chain and the Inhibition Effect by Fibrinogen, Journal of Physical Chemistry B 126 (2022). https://doi.org/10.1021/acs.jpcb.2c05136.

[40] J.R. Brender, K. Hartman, R.P.R. Nanga, N. Popovych, R. de La Salud Bea, S. Vivekanandan, E.N.G. Marsh, A. Ramamoorthy, Role of zinc in human islet amyloid polypeptide aggregation, J Am Chem Soc 132 (2010). https://doi.org/10.1021/ja1007867.

[41] X. Huang, M.P. Cuajungco, C.S. Atwood, R.D. Moir, R.E. Tanzi, A.I. Bush, Alzheimer's disease, β-amyloid protein and zinc, in: Journal of Nutrition, 2000. https://doi.org/10.1093/jn/130.5.1488s.

[42] A.I. Bush, W.H. Pettingell, G. Multhaup, M.D. Paradis, J.P. Vonsattel, J.F. Gusella, K. Beyreuther, C.L. Masters, R.E. Tanzi, Rapid induction of Alzheimer Aβ amyloid formation by zinc, Science (1979) 265 (1994). https://doi.org/10.1126/science.8073293.

[43] L.C.S. Erthal, A.F. Marques, F.C.L. Almeida, G.L.M. Melo, C.M. Carvalho, L.C. Palmieri, K.M.S. Cabral, G.N. Fontes, L.M.T.R. Lima, Regulation of the assembly and amyloid aggregation of murine amylin by zinc, Biophys Chem 218 (2016). https://doi.org/10.1016/j.bpc.2016.09.008.

[44] G.S. Filonov, K.D. Piatkevich, L.M. Ting, J. Zhang, K. Kim, V. V. Verkhusha, Bright and stable near-infrared fluorescent protein for in vivo imaging, Nature Biotechnology 2011 29:8 29 (2011) 757–761. https://doi.org/10.1038/nbt.1918.

[45] H. López-Laguna, J.M. Sánchez, J.V. Carratalá, M. Rojas-Peña, L. Sánchez-García, E. Parladé, A. Sánchez-Chardi, E. Voltà-Durán, N. Serna, O. Cano-Garrido, S. Flores, N. Ferrer-Miralles, V. Nolan, A. de Marco, N. Roher, U. Unzueta, E. Vazquez, A. Villaverde, Biofabrication of functional protein nanoparticles through simple His-tag engineering, ACS Sustain Chem Eng 9 (2021). https://doi.org/10.1021/acssuschemeng.1c04256.

[46] S.S. Flores, P.D. Clop, J.L. Barra, C.E. Argaraña, M.A. Perillo, V. Nolan, J.M. Sánchez, His-tag β-galactosidase supramolecular performance, Biophys Chem 281 (2022) 106739. https://doi.org/10.1016/J.BPC.2021.106739.

[47] P. Álamo, E. Parladé, H. López-Laguna, E. Voltà-Durán, U. Unzueta, E. Vazquez, R. Mangues, A. Villaverde, Ion-dependent slow protein release from in vivo disintegrating micro-granules, Https://Doi.Org/10.1080/10717544.2021.1998249 28 (2021) 2383–2391. https://doi.org/10.1080/10717544.2021.1998249.

[48] E. Vazquez, M. Roldán, C. Diez-Gil, U. Unzueta, J. Domingo-Espín, J. Cedano, O. Conchillo, I. Ratera, J. Veciana, X. Daura, N. Ferrer-Miralles, A. Villaverde, Protein nanodisk assembling and intracellular trafficking powered by an arginine-rich (R9) peptide, Nanomedicine 5 (2010). https://doi.org/10.2217/nnm.09.98.

[49] R.H. Jacobson, X.J. Zhang, R.F. Dubose, B.W. Matthews, Three-dimensional structure of β-galactosidase from E. coli., Nature 1994 369:6483 369 (1994) 761–766. https://doi.org/10.1038/369761a0.

[50] J. Abramson, J. Adler, J. Dunger, R. Evans, T. Green, A. Pritzel, O. Ronneberger, L. Willmore, A.J. Ballard, J. Bambrick, S.W. Bodenstein, D.A. Evans, C.C. Hung, M. O'Neill, D. Reiman, K. Tunyasuvunakool, Z. Wu, A. Žemgulytė, E. Arvaniti, C. Beattie, O. Bertolli, A. Bridgland, A. Cherepanov, M. Congreve, A.I. Cowen-Rivers, A. Cowie, M. Figurnov, F.B. Fuchs, H. Gladman, R. Jain, Y.A. Khan, C.M.R. Low, K. Perlin, A. Potapenko, P. Savy, S. Singh, A. Stecula, A. Thillaisundaram, C. Tong, S. Yakneen, E.D. Zhong, M. Zielinski, A. Žídek, V. Bapst, P. Kohli, M. Jaderberg, D. Hassabis, J.M. Jumper, Accurate structure prediction of biomolecular interactions with AlphaFold 3, Nature 2024 630:8016 630 (2024) 493–500. https://doi.org/10.1038/s41586-024-07487-w.

[51] E.F. Pettersen, T.D. Goddard, C.C. Huang, E.C. Meng, G.S. Couch, T.I. Croll, J.H. Morris, T.E. Ferrin, UCSF ChimeraX: Structure visualization for researchers, educators, and developers, Protein Sci 30 (2021) 70–82. https://doi.org/10.1002/PRO.3943.

[52] E.M.M. MANDERS, F.J. VERBEEK, J.A. ATEN, Measurement of co-localization of objects in dual-colour confocal images, J Microsc 169 (1993) 375–382. https://doi.org/10.1111/J.1365-2818.1993.TB03313.X.

[53] J.H. Mcdonald, K.W. Dunn, Statistical tests for measures of colocalization in biological microscopy, J Microsc 252 (2013) 295–302. https://doi.org/10.1111/JMI.12093.

[54] E. Parladé, J.M. Sánchez, H. López-Laguna, U. Unzueta, A. Villaverde, E. Vázquez, Protein features instruct the secretion dynamics from metal-supported synthetic amyloids, Int J Biol Macromol 250 (2023) 126164. https://doi.org/10.1016/J.IJBIOMAC.2023.126164.

[55] A. Mitraki, J. King, Protein Folding Intermediates and Inclusion Body Formation., Bio/Technology 1989 7:7 7 (1989) 690–697. https://doi.org/10.1038/nbt0789-690.

[56] O. Cano-Garrido, E. Rodríguez-Carmona, C. Díez-Gil, E. Vázquez, E. Elizondo, R. Cubarsi, J. Seras-Franzoso, J.L. Corchero, U. Rinas, I. Ratera, N. Ventosa, J. Veciana, A. Villaverde, E. García-Fruitós, Supramolecular organization of protein-releasing functional amyloids solved in bacterial inclusion bodies, Acta Biomater 9 (2013) 6134–6142. https://doi.org/10.1016/J.ACTBIO.2012.11.033.

[57] N. González-Montalbán, E. García-Fruitós, A. Villaverde, Recombinant protein solubility - does more mean better?, Nat Biotechnol 25 (2007) 718–720.

[58] P. Giannozzi, K. Jansen, G. La Penna, V. Minicozzi, S. Morante, G. Rossi, F. Stellato, Zn induced structural aggregation patterns of β-amyloidpeptides by first-principle simulations and XAS measurements, Metallomics 4 (2012) 156–165. https://doi.org/10.1039/C2MT00148A.

[59] P. Nedumpully-Govindan, Y. Yang, R. Andorfer, W. Cao, F. Ding, Promotion or Inhibition of Islet Amyloid Polypeptide Aggregation by Zinc Coordination Depends on Its Relative Concentration, Biochemistry 54 (2015) 7335–7344. https://doi.org/10.1021/ACS.BIOCHEM.5B00891/SUPPL_FILE/BI5B00891_SI_001.PDF.

[60] M. Rana, A.K. Sharma, Cu and Zn interactions with Aβ peptides: consequence of coordination on aggregation and formation of neurotoxic soluble Aβ oligomers, Metallomics 11 (2019) 64–84. https://doi.org/10.1039/C8MT00203G.

[61] S. Liu, M. Bilal, K. Rizwan, I. Gul, T. Rasheed, H.M.N. Iqbal, Smart chemistry of enzyme immobilization using various support matrices – A review, Int J Biol Macromol 190 (2021) 396–408. https://doi.org/10.1016/J.IJBIOMAC.2021.09.006.

[62] O. Barbosa, C. Ortiz, Á. Berenguer-Murcia, R. Torres, R.C. Rodrigues, R. Fernandez-Lafuente, Glutaraldehyde in bio-catalysts design: a useful crosslinker and a versatile tool in enzyme immobilization, RSC Adv 4 (2013) 1583–1600. https://doi.org/10.1039/C3RA45991H.

[63] L.S. Wong, F. Khan, J. Micklefield, Selective covalent protein immobilization: Strategies and applications, Chem Rev 109 (2009) 4025–4053. https://doi.org/10.1021/CR8004668/ASSET/CR8004668.FP.PNG_V03.

[64] R.A. Sheldon, Cleas, combi-cleas and 'smart' magnetic cleas: Biocatalysis in a bio-based economy, Catalysts 9 (2019). https://doi.org/10.3390/catal9030261.

[65] S. Wu, L. Luo, H. Luo, L. Qiao, H. Chen, M. Li, X. Pei, T. Xie, A. Wang, R.A. Sheldon, Combining Protein Phase Separation and Bio-orthogonal Linking to Coimmobilize Enzymes for Cascade Biocatalysis, Small (2024). https://doi.org/10.1002/smll.202404018.

[66] H. López-Laguna, E. Voltà-Durán, E. Parladé, A. Villaverde, E. Vázquez, U. Unzueta, Insights on the emerging biotechnology of histidine-rich peptides, Biotechnol Adv 54 (2022) 107817. https://doi.org/10.1016/J.BIOTECHADV.2021.107817.

[67] V.D. Jäger, R. Lamm, R. Kloß, E. Kaganovitch, A. Grünberger, M. Pohl, J. Büchs, K.-E. Jaeger, U. Krauss, A Synthetic Reaction Cascade Implemented by Colocalization of Two Proteins within Catalytically Active Inclusion Bodies, ACS Synth Biol 7 (2018) 2282–2295. https://doi.org/10.1021/acssynbio.8b00274.

[68] H. López-Laguna, E. Parladé, P. Álamo, J.M. Sánchez, E. Voltà-Durán, N. Serna, L. Sánchez-García, O. Cano-Garrido, A. Sánchez-Chardi, A. Villaverde, R. Mangues, U. Unzueta, E. Vázquez, H. López-Laguna, E. Parladé, J.M. Sánchez, E. Voltà-Durán, N. Serna, L. Sánchez-García, A. Villaverde, E. Vázquez, P. Álamo, U. Unzueta, R. Mangues, In Vitro Fabrication of Microscale Secretory Granules, (2021). https://doi.org/10.1002/adfm.202100914.